the plant journal

SEB SOCIETY FOR EXPERIMENTAL BIOLOGY

The Plant Journal (2024) **118,** 1719–1731 doi: 10.1111/tpj.16756

Young guard cells function dynamically despite low mechanical anisotropy but gain efficiency during stomatal maturation in *Arabidopsis thaliana*

Leila Jaafar[1,†], Yintong Chen[1,†], Sedighe Keynia[2], Joseph A. Turner[2] and Charles T. Anderson[1,*]

[1]*Department of Biology and Intercollege Graduate Degree Program in Molecular Cellular and Integrative Biosciences, Pennsylvania State University, University Park, Pennsylvania, USA, and*

[2]*Department of Mechanical and Materials Engineering, University of Nebraska-Lincoln, Lincoln, Nebraska, USA*

Received 1 October 2023; revised 12 March 2024; accepted 22 March 2024; published online 3 April 2024.
*For correspondence (e-mail cta3@psu.edu).
†These authors contributed equally to this work.

SUMMARY

Stomata are pores at the leaf surface that enable gas exchange and transpiration. The signaling pathways that regulate the differentiation of stomatal guard cells and the mechanisms of stomatal pore formation have been characterized in *Arabidopsis thaliana*. However, the process by which stomatal complexes develop after pore formation into fully mature complexes is poorly understood. We tracked the morphogenesis of young stomatal complexes over time to establish characteristic geometric milestones along the path of stomatal maturation. Using 3D-nanoindentation coupled with finite element modeling of young and mature stomata, we found that despite having thicker cell walls than young guard cells, mature guard cells are more energy efficient with respect to stomatal opening, potentially attributable to the increased mechanical anisotropy of their cell walls and smaller changes in turgor pressure between the closed and open states. Comparing geometric changes in young and mature guard cells of wild-type and cellulose-deficient plants revealed that although cellulose is required for normal stomatal maturation, mechanical anisotropy appears to be achieved by the collective influence of cellulose and additional wall components. Together, these data elucidate the dynamic geometric and biomechanical mechanisms underlying the development process of stomatal maturation.

Keywords: stomata, guard cells, stomatal maturation, cell wall anisotropy, cellulose, stomatal dynamics, *Arabidopsis thaliana*.

Linked article: This paper is the subject of a Research Highlight article. To view this Research Highlight article visit https://doi.org/10.1111/tpj.16817.

INTRODUCTION

The stomate is a dynamic system at the leaf surface that regulates gas exchange and water relations. Stomatal complexes at their simplest are composed of two guard cells separated at the center of their common boundary by a pore. Guard cells reversibly deform to regulate the size of the stomatal pore in response to environmental stimuli such as changes in light, temperature, humidity, water content, and CO_2 levels. The responses of guard cells to opening- and closure-inducing conditions have been extensively studied in *Arabidopsis thaliana* (Arabidopsis) (Engineer et al., 2016; Kinoshita et al., 2001, 2003). The cell walls of Arabidopsis stomata contain circumferentially organized cellulose, which limits the radial expansion of these cells, causing them to elongate in response to opening stimuli (Rui & Anderson, 2016; Yi et al., 2022). Under opening conditions, yielding of the guard cell wall is accompanied by an increase in turgor pressure as water enters the cell (Yi et al., 2022). These combined processes cause the guard cells, which are longitudinally constrained by polar stiffening of the stomatal complex (Carter et al., 2017), to elongate and bend, leading to widening of the stomatal complex and pore opening. In contrast, under closure conditions, guard cells deflate and their cell walls contract, leading to cell shortening and straightening and closure of the pore (DeMichele & Sharpe, 1973; Franks & Farquhar, 2007; Rui & Anderson, 2016).

Stomatal development can be divided into three phases: differentiation from epidermal stem cells, which terminates with the division of a guard mother cell into

two nascent guard cells; pore formation, in which the recently divided sister guard cells partially separate at the midpoint of their common boundary to generate a stomatal pore; and finally, maturation in which both the pore and the guard cells enlarge and change shape to establish the final structure of the stomatal complex. The first phase has been characterized in detail in Arabidopsis (Guo et al., 2021; Lopez-Anido et al., 2021). Protodermal cells first undergo a series of division and differentiation events that give rise to meristemoid mother cells. Under the influence of the transcription factor SPEECHLESS (SPCH), a meristemoid mother cell divides asymmetrically to give rise to a meristemoid cell and a stomatal lineage ground cell. The MUTE transcription factor then drives the conversion of the meristemoid cell into a guard mother cell that divides symmetrically into two sister guard cells under the influence of a third transcription factor, FAMA (Guo et al., 2021). At this stage, the guard cells share a cell wall that connects them in the middle.

In the second phase of stomatal development, sister guard cells partially separate to form a pore that facilitates gas exchange and water transpiration. During pore formation, pectin degradation occurs at the initiation site of the pore (Rui et al., 2019). Then, the pore enlarges, which requires an increase in turgor pressure. This second phase is followed by stomatal maturation in which guard cells and the pore grow to reach their final size and, hypothetically, their optimal functional state. One challenge for stomatal complexes is that they must continuously function while maturing to enable gas exchange and photosynthesis. However, the cell biological and biomechanical processes underlying stomatal development after pore formation are not well understood.

Stomatal mechanics are governed, in part, by the cell wall that surrounds each guard cell, but evidence suggests that cell wall synthesis continues after stomatal pore formation (Fujita & Wasteneys, 2014; Rui & Anderson, 2016). Atomic force microscope (AFM) measurements have demonstrated that guard cells in *A. thaliana* become stiffer as they mature, with the poles becoming stiffer than the rest of the complex (Carter et al., 2017). The cell walls of guard cells are mechanically anisotropic (Keynia et al., 2023), which helps explain their anisotropic deformations in response to opening and closure stimuli. However, how the wall thickness and 3D biomechanics of guard cells change over the course of stomatal maturation remains unknown.

Here, we used time-lapse live-cell microscopy to establish morphogenetic milestones for stomatal maturation in the cotyledons of *A. thaliana* seedlings, finding that guard cells alter their growth patterns from dorsoventrally symmetrical elongation to establish the final pore size to asymmetric elongation to reach the final complex dimensions. A series of 3D nanoindentation experiments showed that, unlike young guard cells, mature guard cells display mechanical wall anisotropy, being relatively stiffer in the circumferential than longitudinal direction. Additionally, turgor pressure is lower in mature guard cells than in young ones in both closed and open states and changes less between these states. Our model predicts that mature stomatal complexes open more efficiently than young ones. Functional analysis of young and mature cellulose-deficient stomata showed that even though cellulose is required for normal stomatal function, its patterned deposition might not be the only driver that establishes mechanical wall anisotropy in mature guard cells. Together, these results expand our understanding of how stomatal biomechanics are established for the efficient regulation of photosynthesis and water transport in plants.

RESULTS

Stomata mature through a series of morphogenetic milestones, with the pore ceasing growth before the complex

To map the maturation of stomata, we selected individual stomatal complexes that had initiated pore formation in cotyledons of 4-day-old Col-0 seedlings expressing the plasma membrane marker LTI6b-GFP and followed their growth over the next 5 days using confocal microscopy (Figure 1A). Stomatal complex length (b) (Figure 1B), pore length (a) (Figure 1C), junction length ($b - a$) (Figure 1D) and the ratio of pore length-to-junction length ($a/(b - a)$) (Figure 1A,E; Figure S1) were determined over the course of 4 days of maturation. As time progressed, the geometric features of stomatal complexes (complex length, pore length, and pore-to-junction length ratio) increased until

Figure 1. Stomata mature through a series of morphogenetic milestones.
(A) Representative images of the same stomatal complex were imaged every day in Col-0 LTI6b-GFP seedlings from day 4 till day 8 after sowing. Bar = 25 μm.
(B–E) Plots of complex length (B), pore length (C), Junction length (D), and Pore: junction length ratio ($a/(b - a)$) (E) to the days after sowing using data collected from stomata that were done forming their pores in 4-day-old seedlings of *Arabidopsis thaliana*. N = 5 stomata from three seedlings. Bars represent SD.
(F) Regression of one-phase association decay results based on (B–E).
(G, H) Plot of complex length (G) and pore length (H) to junction ratio. n = 154 stomata from six seedlings.
(I) Plot of ratio rate = ((ratio on day n) − (ratio on day $n - 1$))/1 day, pore length rate = ((pore length on day n) − (pore length on day $n - 1$))/1 day, and complex length rate = ((complex length on day n) − (complex length on day $n - 1$))/1 day using data collected from stomata at all developmental stages. n = 154 stomata from six seedlings.
(J) Illustration describing the identified morphogenetic milestones of stomata maturation.

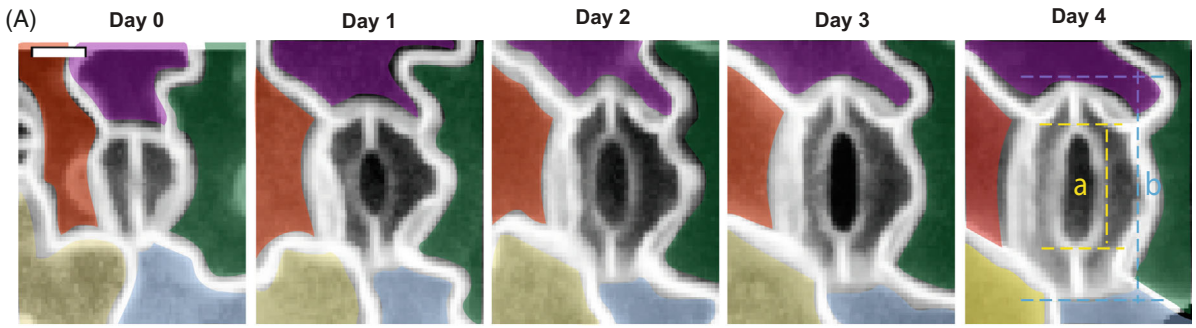

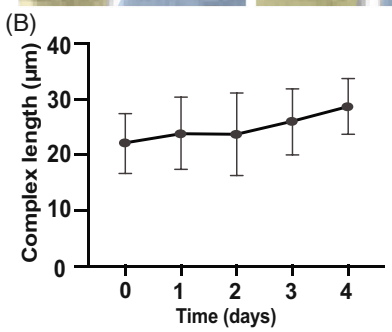

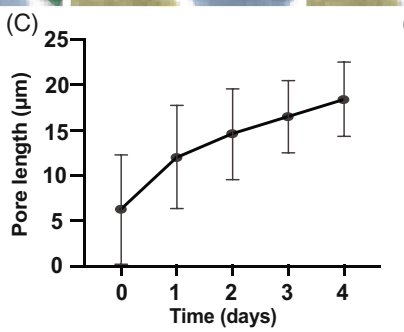

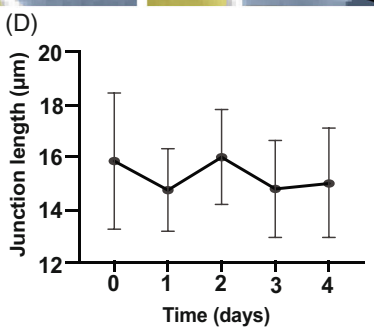

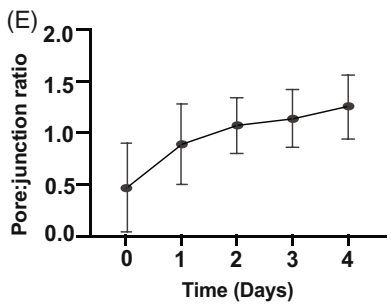

(F)

Regression of One-Phase Association Decay

	Plateau	Half-time	Rate constant
Pore length	16.13	0.75	0.57
Complex Length	32.57	0.97	0.47
Pore : Junction ratio	1.03	0.67	0.69

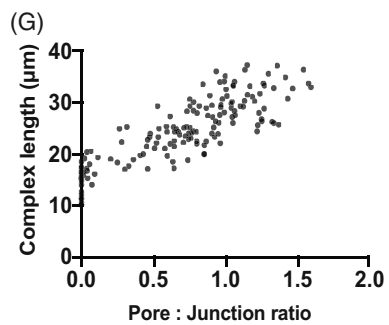

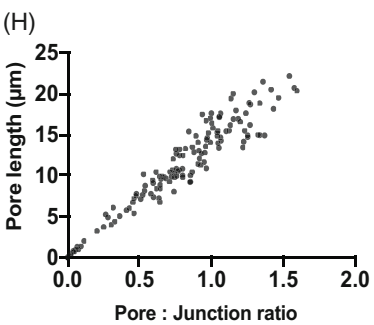

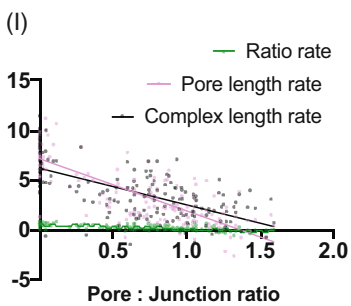

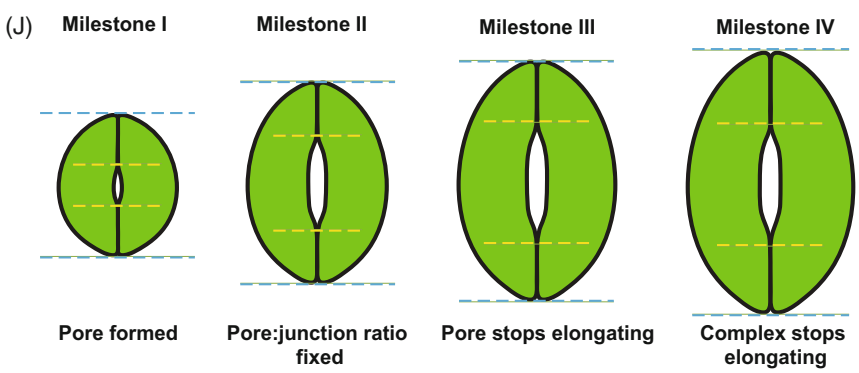

they reached a plateau. A one-phase association was applied to the plots of each feature as a function of seedling age to determine the timeline of the geometric milestones for stomatal maturation (Figure 1F). The results showed that stomatal maturation is marked by four milestones; after pore formation (I), the pore enlarges as the whole complex increases in length until the pore-to-junction ratio becomes fixed around 1.03 (II), then after some continued elongation of both the pore and the complex, the pore stops elongating (III). Finally, the entire complex stops growing (IV) at a length of around 32 μm (Figure 1F). This model is based on regression plots of complex and pore lengths to the pore-to-junction ratio for 154 stomatal complexes (Figure 1G–I). To differentiate between young and mature stomata in later experiments, we established a threshold of a pore-to-junction length ratio of 1 based on the association analysis results (Figure 1F–I). Even though growth is a continuum, we divided developing stomata into two groups, young and mature to test their corresponding behavioral and mechanical properties for experimental simplicity. A stomatal complex with a pore: junction ratio <1 is denoted young, whereas a stomatal complex with a pore: junction ratio >1 is denoted mature.

Guard cell walls thicken and gain mechanical anisotropy and turgor pressure declines during maturation

Thickening and stiffening of the cell wall at the poles of guard cells have been reported to fix the length of the stomatal complex while guard cells elongate or contract during stomatal opening and closure, respectively (Carter et al., 2017). We hypothesized that during cell maturation, other regions of the guard cell wall might thicken as well. To test whether the cell wall thickens as stomata mature, we measured wall thickness from Calcofluor white-stained confocal images of young and mature guard cells in Col-0 cotyledons (Figure S2a). Cross-sectional views of young and mature stomatal complexes revealed overall thicker walls in mature guard cells, with a significant increase in the thickness of the inner periclinal wall (Figure S2).

We have developed 3D nanoindentation as a tool to study the mechanical properties of wild-type and mutant guard cell walls in Arabidopsis (Chen et al., 2021; Keynia et al., 2023). To analyze the mechanical properties of guard cells, nanoindentation can be performed to measure guard cell stiffness in normal, longitudinal, and circumferential directions at shallow and deep indentation depths (Figure S3). Then, these measurements can be combined with image-based measurements of individual complex geometry to build computational finite element (FE) models to determine wall modulus in different directions and turgor pressure for each measured guard cell that match the experimental nanoindentation measurements (Keynia et al., 2023). The experimental longitudinal (Figure 2a) and circumferential (Figure 2b) cell stiffness at shallow (300 nm) and deep (1250 nm) indentation depths show differences in young and mature guard cells (n = 10 guard cells for each maturity level). Several mechanical factors contribute to measured cell stiffness: cell wall properties, cell geometry, boundary properties, and turgor pressure. To determine the wall properties and turgor pressure change that matches the experimental data, FE models of young and mature guard cells were used (Figure 2c).

Comparing wall modulus in the E1 (longitudinal) and E2 (circumferential) directions in young and mature stomata can provide insights into the mechanical changes guard cells undergo during maturation. We used FE analysis to predict the longitudinal (E1) and circumferential (E2) wall moduli of young and mature guard cells (Figure 2c,d). We observed that as the guard cell matures, the longitudinal wall modulus (E1) remains relatively constant while the circumferential modulus (E2) roughly doubles, leading to a substantial increase in the circumferential: longitudinal modulus ratio (E2:E1) (Figure 2d,e). Higher wall modulus in one direction than the other implies enhanced mechanical anisotropy and differential mechanical responses to changes in turgor pressure, with high circumferential modulus constraining guard cell widening during stomatal opening.

In addition to cell wall properties, 3D nanoindentation-FE method approach derives turgor pressure changes (ΔP) upon transitioning from closed to open stomatal states. The results showed that mature guard

Figure 2. Mature guard cells display wall mechanical anisotropy and lower change in turgor pressure compared to young complexes.
(a, b) Experimental apparent wall stiffness of young and mature guard cells in the longitudinal (a) and circumferential (b) directions for shallow (300 nm) and deep (1250 nm) indentation depths. n = 10 young and mature guard cells.
(c) Model of young and mature stomata defining the longitudinal (E1) and circumferential (E2) modulus directions.
(d) Finite element (FE) model estimations of young modulus of young and mature guard cell walls in longitudinal (E1) and circumferential (E2) directions.
(e) Calculated young and mature guard cell wall modulus ratios (E2:E1).
(f) FE estimations of change in turgor pressure (ΔP) in young and mature stomata from closed to open states.
(g) FE model predictions of the change in pore width (μm) young (green) and mature (gray) stomata as a function of the exerted external work (mJ).
(h) Representative images of incipient plasmolysis outcome of young (upper) and mature (lower) stomata. Magenta and green panels correspond to the cell wall (Calcofluor white) and plasma membrane (GFP-LTI6B). Yellow lines correspond to the boundaries of the cell wall (solid yellow) and cell membrane (dashed yellow) which point to locations of membrane retraction from the cell wall (plasmolysis). Bar = 20 μm.
(i) Turgor pressure estimations from incipient plasmolysis assay results of young and mature guard cells in dark (closed) and light (open) conditions. Values are presented as mean ± SE. n = 64 stomata from at least 12 seedlings. Upper ($P < 0.005$) and lower ($P < 0.03$) case letters present significance obtained from two Student's t-tests. *$P < 0.05$, ANOVA.

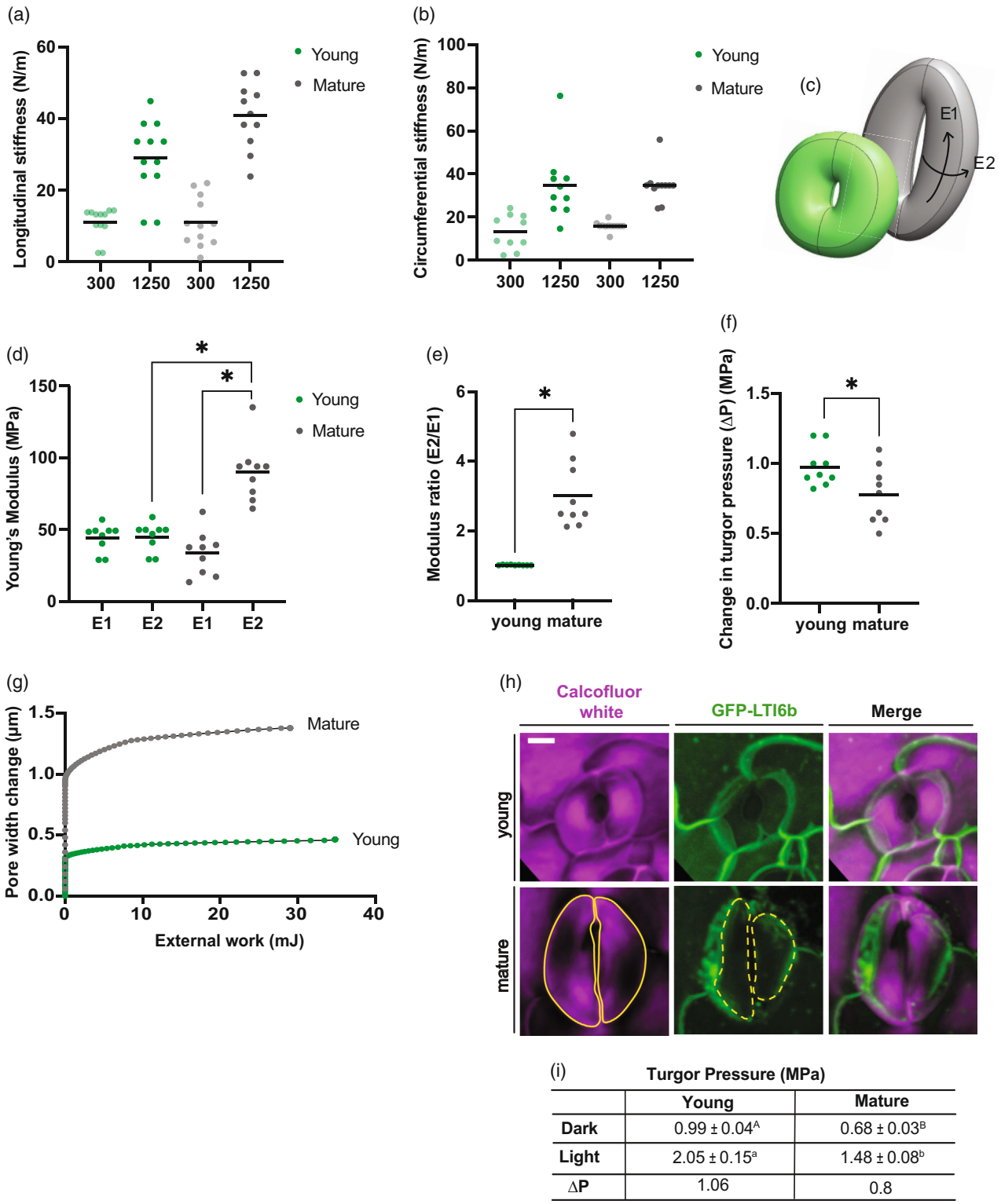

(i) **Turgor Pressure (MPa)**

	Young	Mature
Dark	0.99 ± 0.04^{A}	0.68 ± 0.03^{B}
Light	2.05 ± 0.15^{a}	1.48 ± 0.08^{b}
ΔP	1.06	0.8

cells display lower ΔP than young cells (Figure 2f). Turgor pressure predictions were corroborated experimentally by incipient plasmolysis assays (Weber et al., 2015). Incipient plasmolysis is the state at which 50% of cells plasmolyze when subjected to a specific osmolyte concentration. Under the same osmotic solution, in open and closed stomatal states, a higher proportion of mature guard cells plasmolyzed compared to young guard cells (Figure S4).

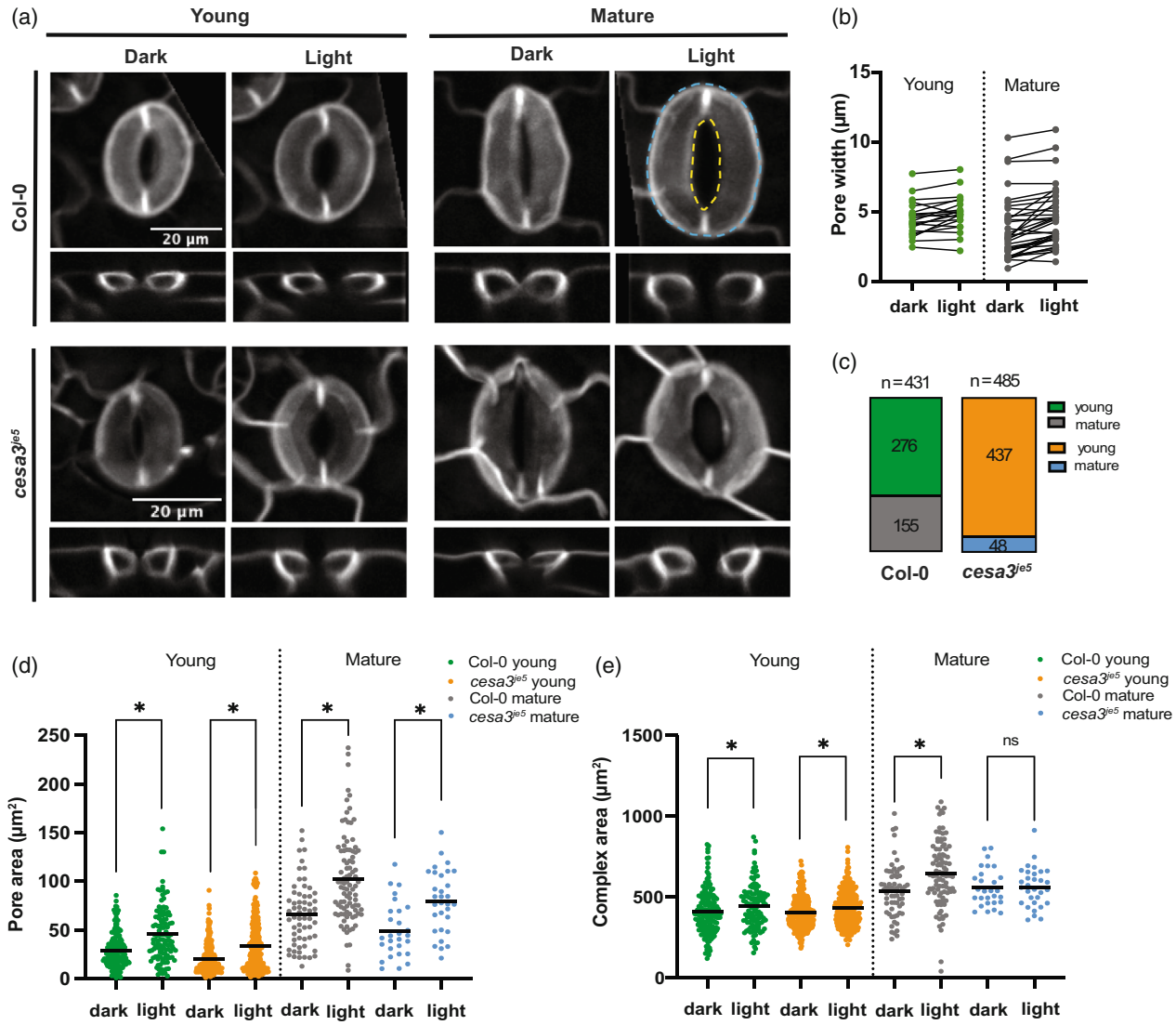

Figure 3. Cellulose-deficient cotyledons exhibit greater percentages of young stomata with smaller relative pore size.
(a) Representative images of *xy* (upper) and *xz* (lower) views of Col-0 and *cesa3*^{je5} young and mature stomata in response to 2.5 h of light treatment. Yellow and blue dashed lines correspond to pore and complex areas, respectively. The signal corresponds to GFP-LTI6b plasma membrane marker. Bar = 20 µm.
(b) Quantification of change in pore width of young (green) and mature (gray) stomata before and after 2.5 h of light treatment. $n > 21$ stomata from eight seedlings.
(c) Distribution of young (green or orange) and mature (gray or blue) stomata in Col-0 and *cesa3*^{je5}. $n = 431$ stomata of Col-0 and $n = 485$ stomata of cesa3^{je5}.
(d, e) Measured pore (d) and complex (e) area of young and mature stomata of Col-0 and cesa3^{je5} in dark and light conditions. $n > 62$ stomata from 12 Col-0 seedlings. $n > 256$ young stomata and $n > 27$ mature stomata from 14 cesa3^{je5} seedlings. ns $P > 0.05$, $^{*}P < 0.05$, Student's *t*-test and Mann–Whitney test.

The estimated turgor pressure in mature guard cells in both open and closed states was lower than that of young guard cells (Figure 2g,h). Additionally, the change in turgor pressure from closed to open states as estimated by incipient plasmolysis was lower in mature guard cells than in young guard cells (Figure 2g); these data are in close agreement with the FE analysis.

Despite displaying different mechanical anisotropic properties, young and mature guard cells respond to opening stimuli by opening the pore (Figure 3b). To identify possible reasons for gaining wall anisotropy by guard cells during maturation, we used our FE models to quantify the energy efficiency of pore opening for both ages. The results showed that mature stomata expend less energy than young stomata (29 mJ) to establish wider stomatal openings (1.377 µm) (Figure 2g). These findings indicate that guard cells gain mechanical anisotropy in their cell walls as they mature, enabling them to achieve stomatal opening at lower turgor pressure while using less energy.

In wild-type seedlings, mature stomata open to a greater degree than young stomata

To determine the effects of higher wall anisotropy and lower turgor pressure on stomatal function, we first imaged young and mature stomatal complexes in cotyledons of Col-0 LTI6B-GFP seedlings that had been placed in the dark overnight, then subjected the seedlings to 2.5 h of light to induce stomatal opening and imaged the same stomatal complexes, measuring geometric changes in their stomata (Figure 3). As expected, light conditions led to stomatal opening and thus an increase in pore and complex area of both young and mature stomata (Figure 3a,b,d,e; Figure S6). This implies that stomatal response to opening stimuli is maintained across developmental stages. However, mature stomata displayed a greater pore: complex area ratio in dark and light conditions than young stomata (Figure S6). This means that in Col-0, the pore occupies a larger portion of mature complexes than of young ones. Additionally, comparing the pore: complex area ratio gives insight into the degree of change in pore area with respect to complex area upon transition from closed to open stomatal states. Pore: complex area ratio did not change substantially between closed and open states in young stomata, whereas in mature stomata, this ratio increased significantly (Figure S6). Hence, although stomata at different developmental stages behave similarly in response to opening conditions, mature stomata evince a greater degree of opening, which hints at an enhanced stomatal function in regulating physiological processes such as gas exchange and water relations.

Cellulose is required for normal stomatal maturation and achieving maximum stomatal opening

Cellulose is a major load-bearing polymer in the cell wall and has been shown to facilitate guard cell elongation in response to light (Rui & Anderson, 2016). We hypothesized that the organized deposition of cellulose microfibrils might be a driver of the mechanical anisotropy in the guard cell wall predicted by nanoindentation and modeling (Figure 2). To test this hypothesis, we determine the responses of young and mature stomata of the cellulose-deficient mutant *cesa3*^{je5} to light. Similar to wild type, and despite lower cellulose content in *cesa3*^{je5}, young and mature guard cells responded to light by opening their pores (Figure 3a,d; Figure S6). Interestingly, unlike wild-type controls, mature stomatal complexes of *cesa3*^{je5} seedlings did not show a significant change in total area when going from dark to light conditions even though their pores opened (Figure 3d, e). Furthermore, young and mature *cesa3*^{je5} stomata displayed smaller pores and a lower degree of pore opening determined by lower pore: complex area ratios relative to Col-0 (Figure 3a,d; Figure S6). Additionally, optical cross-sections of mature *cesa3*^{je5} guard cells appeared less round than Col-0 controls (Figure 3a). We also observed that the overall number of mature stomata was low in *cesa3*^{je5} (approximately 10%), unlike Col-0 cotyledons where mature stomata presented approximately 36% of the total number of stomata captured (Figure 3c). Unlike previous reports of cellulose in the innermost layer of young guard cells being disorganized (Fujita & Wasteneys, 2014), Pontamine Fast Scarlet 4B (S4B) staining, which reveals cellulose organization throughout the thickness of the wall (Anderson et al., 2010), showed that cellulose microfibrils in young and mature guard cells of Col-0 were wrapped around the cells in a radial pattern (Figure S5). Together these data suggest that cellulose is required for normal stomatal maturation, both in terms of cell geometry and mechanical anisotropy in the wall, but that other wall components likely contribute to the functional architecture of the mature guard cell wall and can partially compensate for defects in cellulose content.

DISCUSSION

In *A. thaliana*, the symmetric division of the Guard Mother Cell into two guard cells is driven by transcription factors (FAMA and FOUR LIPS) (Guo et al., 2021). After cell division, the stomatal pore is formed and enlarged by pectin degradation and increased cell turgor, respectively (Rui et al., 2019). Little is known about the mechanisms underlying stomatal maturation after pore formation. Here, we identified geometric and mechanical changes that occur during guard cell maturation and their influence on stomatal function.

We started by determining the chronological order of geometric changes of the stomatal complex when transitioning from young to mature states (Figure 1). We tracked the same complexes for 4 days after pore formation and assessed changes in their geometric features including complex, pore, and junction lengths (Figure 1A–D). Then, we fitted the geometric measurements into a one-phase association model as a function of seedling age to establish a stomatal maturation timeline (Figure 1G–I). The model revealed four morphogenetic milestones of stomatal maturation (Figure 1J). After pore formation (Milestone I), the guard cells grow until the pore and junctions are similar in length (pore: junction length ratio approximately 1.03) (Milestone II). Guard cells continue elongating symmetrically until the inner periclinal cell region stops to fix the pore length (Milestone III). Finally, guard cells expand asymmetrically where the outer periclinal cell region expands to increase the complex length, then stops when it reaches the size of a fully mature stomatal complex (Milestone IV). The samples were repeatedly moved from the growth chamber to the microscope and back for sequential observation. However, the consistent results from different seedlings help overcome the variability that might be introduced by this experimental design.

Microscopy evidence shows that as guard cells mature, their cell walls thicken and become organized radially (Fujita & Wasteneys, 2014; Zhao & Sack, 1999), potentially driving the longitudinal expansion of guard cells in response to opening stimuli and constraining their circumferential widening. While young guard cells display similar wall thickness around the cell diameter, the inner periclinal wall is thicker than the outer periclinal wall in mature guard cells, consistent with prior measurements of wall thickness using transmission electron microscopy (Keynia et al., 2023) and we also observed thicker walls in the ventral anticlinal region of mature guard cells (Figure S2). AFM measurements across the width of the stomatal complex have shown that the anticlinal wall facing the pore is stiffer than the dorsal anticlinal wall of mature guard cells, unlike in young complexes that showed lower, roughly equal stiffness values across both regions (Carter et al., 2017). The asymmetric guard cell expansion that occurs from Milestones III to IV, where the pore stops elongating but the guard cells continue to elongate, might be explained by the increased thickness and stiffness of the ventral anticlinal wall in mature guard cells that would resist elongation in response to increasing turgor pressure during growth (Carter et al., 2017). Hence, if a thicker ventral anticlinal wall is not necessary for guard cell opening as reported by Carter et al. (2017), it might instead be important for establishing the mature stomatal form and optimizing the efficiency of stomatal dynamics.

Previous reports highlighted the importance of computational models to determine the mechanical properties of biological systems (Boudon et al., 2015; Forouzesh et al., 2013; Hayot et al., 2012; Li et al., 2022; Woolfenden et al., 2017). We used nanoindentation coupled with FE modeling to characterize the mechanical traits of young and mature guard cells, including cell wall moduli in different directions and turgor pressure (Figure 2). Normal indentation at different depths provides the stiffness properties of the material in a direction perpendicular to the surface of the cell. However, lateral indentation yields in-plane mechanical aspects of the wall in different directions, which refines our understanding of the guard cell wall as a dynamic entity and provides insight into variations in turgor pressure (Keynia et al., 2023). We also used this measurement and modeling framework to calculate the work required to open stomata of different maturation states.

Using lateral nanoindentation in the longitudinal and circumferential directions, we determined cell stiffness in young and mature stomatal complexes at different depths (Figure 2a,b; Figure S3). To differentiate between the mechanical factors contributing to cell stiffness, we built FE models based on the geometry of young and mature guard cells, followed by an iterative process to match the modeled pore size to experimental data. The results show that while young guard cells display similar wall moduli in all directions (E2/E1 $\approx$ 1), mature guard cell walls present higher circumferential than longitudinal modulus (E2/E1 > 2) (Figure 2c–e). This finding suggests that guard cells acquire anisotropic wall properties as they mature. We speculate that wall anisotropy in mature guard cells arises from the radial arrangement of the cellulose microfibrils (Fujita & Wasteneys, 2014; Rui & Anderson, 2016). In addition to determining cell wall properties, we employed our approach to determine turgor pressure values (Figure 2f). The models showed a significantly smaller increase in turgor pressure change (ΔP) upon pore opening in mature guard cells than in young guard cells (Figure 2f). These results were comparable to estimations of turgor pressure based on incipient plasmolysis experiments (Figure 2g,h). One caveat of the nanoindentation and FE modeling approach is the degree to which the measurements of guard cells are influenced by mechanical interactions with neighboring epidermal cells; however, given that these neighboring cells did not differ greatly in size between young and mature stomatal complexes, we hypothesize that these interactions should be consistent across our measurements. Although the prescribed boundary conditions reflect the impact of neighboring cells to some degree, future experiments testing the mechanical properties of both guard and neighboring cells (Li et al., 2022) could be used to test this hypothesis.

Measuring pore and complex area of young and mature stomata allowed us to assess their behaviors in response to light (Figure 3). The data show that at all developmental stages, stomata respond to light by opening their pores, which increases pore and complex areas (Figure 3a,b,d,e). These results imply that similar dynamic behaviors are achieved by cells of different sizes and maturation states in response to an opening stimulus. These experiments were performed on cotyledons growing in culture plates (approximately 100% humidity), which might underestimate stomatal response to opening or closing stimuli under less humid conditions. However, the results show a clear difference in young and mature stomatal performance that might be even greater in true leaves. Open pores in mature stomata were larger (Figure 3a,b,d; Figure S6). This could be simply because the mature guard cells are larger in size. However, according to the maturation milestone model (Figure 1J), mature guard cells have a longer inner anticlinal wall, a shorter junction (pore-to--junction length >1), and a greater pore area-to-complex area ratio (Figure S6). Therefore, the pore occupies a greater portion of the mature stomatal complex, which would be expected to enhance gas exchange across the stomatal pore, unlike young complexes that possess smaller pores relative to their complex areas (Figure S6). This increase in pore:complex area might be a key functional feature of stomatal maturation.

Mature guard cells undergo smaller changes in turgor pressure than young guard cells yet open fully in response to opening stimuli. This might be due to the mechanical wall anisotropy gained by mature guard cells, which might aid in achieving maximum pore opening while exerting lower energy (Figure 2g). Previous reports observed a random organization of fibrillar material at the innermost cell wall face in guard cells prior to pore formation and a radial pattern of material in mature guard cells using field emission scanning electron microscopy (FESEM) (Fujita & Wasteneys, 2014); however, microtubules and thus presumably the trajectories of cellulose synthases were observed to be radial in both nascent and mature guard cells (Rui & Anderson, 2016). Hence, we suspect that cellulose is a key driver of mechanical wall anisotropy and anisotropic morphogenesis in mature guard cells. However, in the abovementioned FESEM images of the innermost cell wall layer of young and mature Col-0 stomata, cellulose is not specifically labeled and the sample preparation did not include pectin degradation (Fujita & Wasteneys, 2014). Furthermore, detailed analyses of cellulose synthase particle trajectories have not been performed in young and mature guard cells. Moreover, to our knowledge, a clear morphological boundary between young and mature stomata has not been reported. Therefore, even though the abovementioned images are insightful and provide a useful reference for wall patterning at the innermost layer in different types of cells, we cannot yet make definitive conclusions regarding cellulose arrangement in young and mature guard cells.

Our results with a cellulose synthase mutant provide evidence that cellulose contributes to the mechanical anisotropy of mature guard cells but is not the sole determinant of this anisotropy. The radial arrangement of cellulose in young and mature stomata determined by S4B staining and the ability of cellulose-deficient guard cells to close and open the pores in response to dark and light conditions (Figure 3), means that other cell wall components besides cellulose likely contribute to the mechanical wall anisotropy determined by our approach (Figure 2). Pectin is a major component of the cell wall that contributes to guard cell function (Chen et al., 2021; Rui et al., 2017) and wall anisotropy in mature guard cells (Keynia et al., 2023). Overexpression of polygalacturonase involved in expansion3 (*PGX3*), a pectin-degrading enzyme, affects the speed of stomatal response (Rui et al., 2017), and results in higher mechanical anisotropy in the guard cell wall, whereas knocking out *PGX3* results in lower wall anisotropy as determined by lateral nanoindentation (Keynia et al., 2023). Similar to the *pgx3-1* knock-out mutant, cellulose-deficient mutant *cesa3*^{je5} displayed lower mechanical anisotropy as determined from the nanoindentation-FE model approach. These results imply that mechanical wall anisotropy in mature guard cells is achieved by the combined effects of cellulose and pectins such that the pectin stiffness profile across the guard cell has an orientation dependence. It remains unclear at this time whether the mechanical anisotropy of the pectins coaligns with cellulose via some type of cross-linking or if it is the result of anisotropic deposition and/or deformation of pectin during wall assembly and/or cell expansion, or even the repeated deformation of the guard cell that occurs during stomatal response. Further mechanical studies are needed to identify additional differences between young and mature guard cells of cell wall mutants that can be correlated with altered stomatal function.

In summary, our data depict the morphogenetic and biomechanical milestones of stomatal maturation in *A. thaliana*. After pore formation, the whole complex grows until the pore reaches its maximum length. The guard cells continue to elongate asymmetrically to establish the final mature form of the stomatal complex. Mature guard cells gain mechanical anisotropy in their walls through the organization of cellulose and other wall components. Our modeling results indicate that the acquisition of mechanical anisotropy in the guard cell wall enables an energy-efficient stomatal response to environmental stimuli (Figure 4). Further studies can build on this biomechanical and morphogenetic foundation to dissect additional genetic and molecular factors that influence how efficient stomatal function is maintained and enhanced over the course of the final stage of stomatal development.

MATERIALS AND METHODS

Plant growth conditions

Arabidopsis thaliana Col-0 LTI6B-GFP (Cutler et al., 2000) and *cesa3*^{je5} LTI6B-GFP seeds were sterilized in 30% bleach and 0.1% SDS for 20 min then stratified in 0.15% (w/v) agar at 4°C in the dark for at least 3 days. Seeds were sowed on Murashige and Skoog (MS) plates containing 2.2 g/L MS salts (Caisson Laboratories, North Logan, UT, USA), 0.6 g/L MES, 1% (w/v) sucrose, and 0.8% (w/v) agar (Sigma, St Louis, MO, USA), pH 5.6. Seedlings were grown at 22°C under 24-h light (4100K fluorescent Lamp, 800, 900 PPFD).

Guard cell tracking

We selected stomata that had just formed pores from cotyledons of 4-day-old Col-0 LTI6B-GFP seedlings (Cutler et al., 2000) and tracked their growth for 4 days. Every day, the same seedlings were mounted gently on slides and imaged using a Zeiss Cell Observer SD microscope with a Yokogawa CSU-X1 spinning disk head and a 40× oil objective. Intact seedlings were then returned to the MS plate and allowed to grow for another day before being mounted and imaged again. In each sample, the same region was imaged every day until day 8 after sowing. Complex, pore, and junction lengths, as well as pore: junction ratios were measured and calculated from individual stomatal complexes using ImageJ. We used a 488-nm excitation laser and a 525/50-nm emission filter to detect the GFP signal in all experiments.

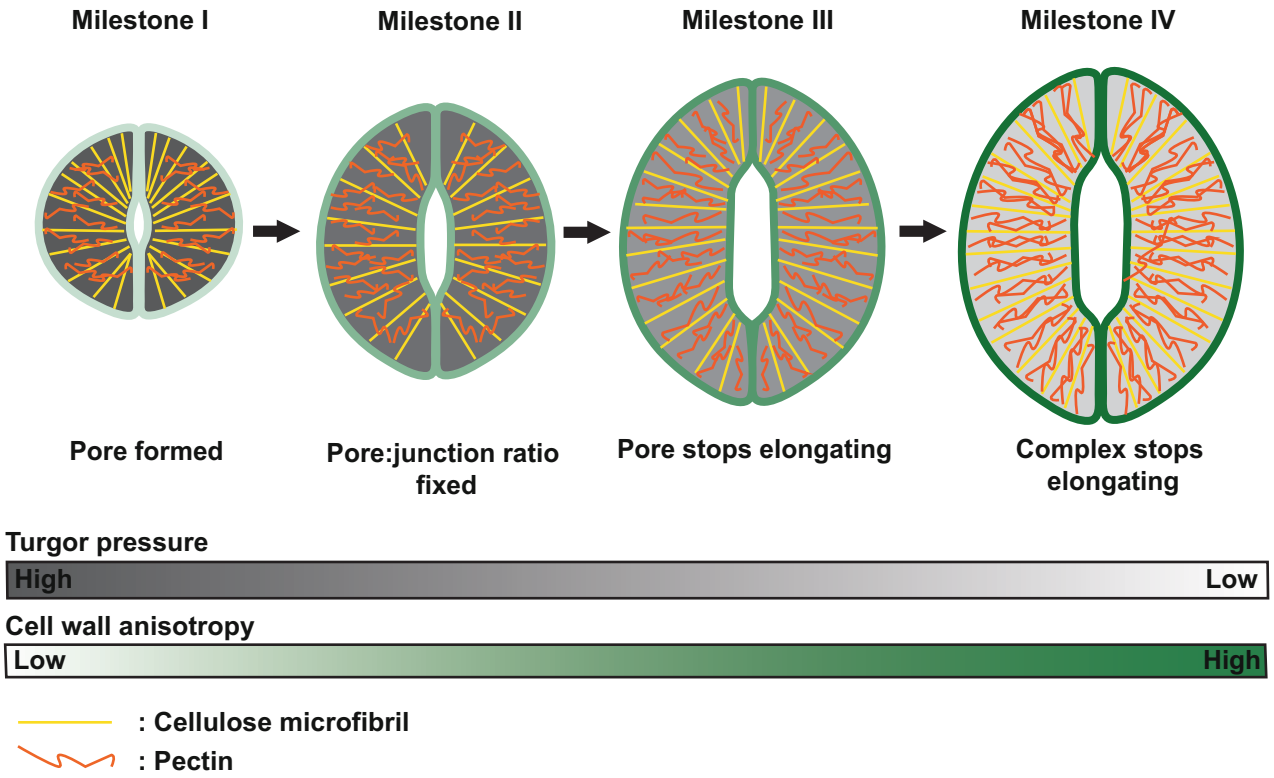

Figure 4. Stomata mature through a series of geometric milestones.
Stomatal maturation starts with the formation of the pore that elongates along with the guard cells until pore: junction ratio gets fixed at >1. Then, the pore stops elongating while the complex grows to achieve the final mature stomatal form. During maturation, guard cell turgor pressure (gray) decreases while cell wall anisotropy (green) is enhanced. This is achieved by the organization of cellulose (yellow lines) and other cell wall components like pectin (orange lines).

Instrumented indentation testing (nanoindentation)

Nanoindentation experiments were conducted using a Hysitron TI Premier Nanoindenter (Bruker, USA), equipped with a 50× objective to target guard cells accurately. The conical-type tip of the probe had a diameter of 2–3 μm, and a 2-μN engaging force was applied to the middle of each cell. The size of the tip in relation to the guard cell and adjacent pavement cells guarantees that there is no contact with the neighboring cells while indenting the center of guard cells. The input load function was defined as the displacement values, with the loading and unloading and the lateral motion rate set to 30 nm/sec. During lateral indentation, the normal displacement was set to zero with respect to the previous position, while for normal indentation, the lateral displacement was set to zero to ensure that the probe would indent the center of the guard cell. The experimental normal and lateral stiffness were measured using nanoindentation as detailed in Keynia et al. (2023) and were subsequently matched in the iterative process of the FE method in order to determine the cell wall moduli and turgor pressure change.

Finite element method modeling

We followed a modeling approach using the FE method reported in Keynia et al. (2023). FE method analysis of nanoindentation measurements was conducted using commercial finite element software (Abaqus, 2019) to estimate the wall modulus and turgor pressure of the cell in young and mature guard cells. At least nine guard cells for each developmental stage were modeled with the finite element method. Using images from a laser confocal microscope, stomatal complex length, guard cell geometry, and pore width were measured, and a model of each guard cell was constructed individually using the lofting method in SolidWorks. The initial pore width used in the FE method analyses was based on the pore width at the closed state for young and mature Col-0 stomata. The thickness distribution of the cross-section of the guard cells was set based on measurements from Calcofluor images, then the structural model was imported into Abaqus. To simulate the nanoindentation measurements, the conical tip was scanned using a confocal microscope and its geometry was also imported into Abaqus. A linear anisotropic elastic model using a discrete coordinate system was assigned uniformly across the whole cell and based on the orientations of cellulose and matrix polysaccharides in the guard cell wall, the anisotropic modulus was assumed to have a relation $E_1 = E_3$ and its value was calculated based on iteration with an appropriate initial guess. E2 defined the wall modulus along the circumferential direction of the cell; the modulus in this direction had the maximum value based on initial assumptions (Fujita & Wasteneys, 2014; Lucas et al., 2006; Rui & Anderson, 2016). Poisson's ratios were set to $\nu_{12} = \nu_{23} = 0.3$ and $\nu_{13} = 0.47$. Shear modulus was assumed to have a relation $G_{12} = G_{23}$, and G_{13} can be determined by $G_{13} = E_1/[2(1 + \nu_{13})]$. Due to lateral indentation, contact properties such as friction coefficient can play a significant role in the stiffness values of the cell wall in lateral directions (x and y) derived from the computational model. To exclude these

parameters from the iteration, lateral indentations starting from 100 nm displacement from the center and increasing up to 5 μm were performed on nine cells along the longitudinal direction to investigate the contact properties between the guard cell and nanoindenter tip during lateral motion. These experiments revealed the point at which sliding begins, the maximum lateral force, and the slope of the lateral force versus normal force (friction coefficient) of non-sliding indentation. As a result, for all the computational models, the friction coefficient was set to 0.3, and the shear stress limit and fractions of characteristic surface dimensions were set to 0.3, 50 MPa, and 0.9, respectively (Keynia et al., 2023). For boundary conditions, the materials at the polar positions were confined, ventral edges were free of constraint, and dorsal edges were constrained in the vertical direction to represent constraints from adjacent pavement cells (Chen et al., 2021). The analysis was conducted in three steps: cell pressurization, normal and lateral nanoindentation. The pore width at the end of the pressurization and the stiffness at shallow and deep indentation depths were used to compare with experimental measurements iteratively (Keynia et al., 2023). Turgor pressure and wall modulus were estimated based on the simulations with consistent pore width and normal and lateral stiffness. External work, in the context of hydrostatic pressure causing cell expansion, refers to mechanical work done by the cell wall as it pushes against an external force (e.g., turgor pressure in neighboring cells) during its expansion and cell opening. The external work was an output from the FE model. The change in turgor pressure for these simulations occurred for a duration that was 10 times the wall viscoelastic time constant assumed for the material model.

Incipient plasmolysis assays

We followed the incipient plasmolysis assay protocol reported by Weber et al. (2015). Briefly, cotyledons were excised from 8-day-old Col-0 LTI6b-GFP seedlings (Cutler et al., 2000) and subjected to light or dark conditions to generate open and closed stomata sample groups, respectively. Cotyledons with open or closed stomata were soaked in 2% (w/v) Calcofluor white (Sigma, St Louis, MO, USA) in sorbitol solutions of different concentrations (0.4, 0.6, and 0.8 M for the open group, and 0.2, 0.3, and 0.4 M for the closed group) for 40 min before imaging using a Zeiss Cell Observer SD microscope with a 63× oil objective. Excitation lasers at 488 and 405 nm with 525/50 and 450/50 nm emission filters were used to detect GFP and Calcofluor white signals, respectively. Quantification and calculation of the percentage of plasmolyzed young and mature stomata were done using ImageJ. The percentage of plasmolyzed cells was plotted as a function of sorbitol concentration to perform linear regression analysis. The sorbitol concentration of incipient plasmolysis was determined (50% of guard cells are plasmolyzed) and used to calculate turgor pressure according to Van't Hoff equation $\Psi = c \cdot R \cdot T$, where c is the concentration of sorbitol, R is the ideal gas constant (8.314 kPa·Lmol^{-1}·K^{-1}), and T is the temperature in Kelvin (298 K). Data were collected from nine seedlings in total in three independent experiments per condition.

Stomatal dynamics assays

To compare the response of young and mature stomata to light, 10-day-old Col-0 LTI6B-GFP seedlings (Cutler et al., 2000) were incubated in the dark for 24 h to induce stomatal closure. Dark-treated cotyledons were excised and Zeiss Cell Observer SD microscope with a Yokogawa CSU-X1 spinning disk head and a 40× oil objective was used to image stomatal complexes. Then, the cotyledons were gently removed from the slide and incubated in stomatal opening solution (50 mM KCl, 0.1 mM $CaCl_2$, and 10 mM MES-KOH, pH 6.15) and light for 2.5 h to induce stomatal opening. The same cotyledons were mounted on slides and the same regions were imaged again to capture stomata in open states. ImageJ was used to measure changes in pore width before and after light treatment. Eight seedlings were imaged in one experiment.

For a population-level assessment of young and mature stomatal function, 8-day-old Col-0 LTI6B-GFP or *cesa3^{ie5} LTI6B-GFP* seedlings subjected to dark overnight then moved to light conditions for 2.5 h to induce stomatal closing and opening, respectively. Excised cotyledons were imaged using Zeiss Cell Observer SD microscope with a Yokogawa CSU-X1 spinning disk head and a 40× oil objective with 488-nm excitation and a 525/50-nm emission filter. ImageJ was used to evaluate pore and complex area of closed or open young and mature stomata. Nine to twelve seedlings were imaged in three independent experiments.

Pontamine fast scarlet 4B (S4B) staining

Eight-day-old Col-0 seedlings were grown in continuous light till day 7 where they were incubated in the dark overnight to induce stomatal closure. Then, seedlings were moved to light conditions for 2.5 h to induce stomatal opening. Cotyledons from seedlings in dark and light conditions were excised and cleared to disrupt the cuticle following the tissue-clearing protocol in Sharma (2017). Briefly, cotyledons were incubated in a clearing solution (7:1 95% ethanol:acetic acid) overnight at room temperature. Then, the clearing solution was removed, and cotyledons were incubated in 1 M KOH for 30 min to 1 h. Cotyledons were then washed twice with water and stained with 0.1% (w/v) S4B (Sigma, St Louis, MO, USA) (Anderson et al., 2010) in liquid MS medium for 30 min at room temperature. Finally, S4B-stained cotyledons were mounted on slides for confocal imaging. Z-stacks were collected using a Zeiss Cell Observer SD microscope with a Yokogawa CSU-X1 spinning disk head and a 100× oil objective and a 561-nm excitation filter. Confocal z-series were recorded with a 0.2-μm step size. Raw confocal z-stacks were deconvoluted in AutoQuant X2 (Media Cybernetics) and maximum projections of the deconvoluted images were obtained using ImageJ.

Cell wall thickness measurements

Eight-day-old Col-0 LTI6b-GFP seedlings (Cutler et al., 2000) were stained with 2% (w/v) Calcofluor white (Sigma, St Louis, MO, USA) for 5 min at room temperature. Z-stack images of young and mature stomata were collected using Zeiss Cell Observer SD microscope with a Yokogawa CSU-X1 spinning disk head and a 63× oil objective. Z-stacks were deconvoluted using AutoQuant X2 and the thickest regions of the outer and inner periclinal walls were measured using ImageJ. Nine seedlings were imaged in three independent experiments.

Statistical analyses

Statistical analysis was done using GraphPad. Dots represent individual data points and lines represent mean value of the set. Sample size, statistical significance annotation (asterisks), and statistical tests corresponding to each plot are described in figure legends.

AUTHOR CONTRIBUTIONS

All authors designed experiments; LJ, YC, and SK performed experiments; all authors analyzed data; LJ drafted the manuscript; all authors reviewed and edited the manuscript.

ACKNOWLEDGMENTS

The authors thank Hojae Yi, James Z. Wang, and Dolzodmaa Davaasuren for helpful discussions. This work was supported by collaborative U.S. National Science Foundation grant MCB-2015943 (CTA)/MCB-2015947 (JAT).

CONFLICT OF INTEREST STATEMENT

The authors declare no conflicts of interest.

DATA AVAILABILITY STATEMENT

All data used in the manuscript are presented in the main and Supplementary figures. Additional raw data are available upon request to the corresponding author.

SUPPORTING INFORMATION

Additional Supporting Information may be found in the online version of this article.

Figure S1. Stomatal maturation trends in Col-0 cotyledons. Tracking stomatal maturation by measuring complex (a), pore (b), and junction lengths (c) over time (days). (d) Calculated pore-to-junction ratio over time (days). $n = 15$ stomata from three seedlings.

Figure S2. Mature guard cells have a thicker inner periclinal cell wall. (a) Calcofluor white staining of young and mature guard cells in *xy* (upper) and *xz* (lower) projections. Yellow and blue boxes highlight the inner and outer periclinal walls, respectively. Bar = 10 μm. (b) Quantification of inner and outer periclinal wall thickness in young (green) and mature (gray) guard cells. $n > 60$ stomata from nine seedlings. ns >0.05, $*P < 0.05$, Student's *t*-test.

Figure S3. Measurements of stiffness of young and mature guard cells using nanoindentation at different depths. (a–c) Apparent stiffness measurements of young guard cells in normal (a), longitudinal (b), and circumferential (c) directions using nanoindentation at various indentation depths (150, 300, 450, and 1250 nm). $n > 10$ guard cells in each category. (d–f) Apparent stiffness measurements of mature guard cells in normal (a), longitudinal (b), and circumferential (c) directions using nanoindentation at various indentation depths (150, 300, 450, and 1250 nm). $n > 10$ cells per category.

Figure S4. Ratios of plasmolyzed young and mature guard cells in closed and open states as a function of sorbitol concentration. (a, b) Quantification of the ratio of plasmolyzed young (a) and mature (b) guard cells at different osmotic concentrations (M) in dark (closed) and light (open) conditions. $n > 64$ guard cells from at least nine seedlings. ns $P > 0.03$, $*P < 0.03$, Student's *t*-test.

Figure S5. Cellulose microfibrils are circumferentially wrapped around young and mature guard cells of Col-0 and cesa3^{je5} stomata. Maximum projections of deconvoluted z-series of S4B-stained young and mature guard cells of Col-0 (left) and cesa3^{je5} (right) seedlings. Bar = 5 μm.

Figure S6. Mature stomata open to a greater degree than young stomata in Col-0 seedlings, and relative pore sizes in young and mature stomata of cesa3^{je5} seedlings (related to Figure 3). (a, b) pore: complex area ratios of young (green or orange) and mature (gray or blue) stomata of Col-0 (a) and cesa3^{je5} (b) seedlings before and after 2.5 h of light treatment. $n = 62$ young and mature stomata from 12 Col-0 seedlings. $n > 255$ young stomata and $n > 28$ mature stomata from 14 cesa3^{je5} seedlings. ns $P > 0.05$, $*P < 0.05$, Student's *t*-test and Mann–Whitney test.

REFERENCES

Anderson, C.T., **Carroll, A.**, **Akhmetova, L.** & **Somerville, C.** (2010) Real-time imaging of cellulose reorientation during cell wall expansion in Arabidopsis roots. *Plant Physiology*, **152**, 787–796.

Boudon, F., **Chopard, J.**, **Ali, O.**, **Gilles, B.**, **Hamant, O.**, **Boudaoud, A.** ***et al.*** (2015) A computational framework for 3D mechanical modeling of plant morphogenesis with cellular resolution. *PLoS Computational Biology*, **11**, e1003950.

Carter, R., **Woolfenden, H.**, **Baillie, A.**, **Amsbury, S.**, **Carroll, S.**, **Healicon, E.** ***et al.*** (2017) Stomatal opening involves polar, not radial, stiffening of guard cells. *Current Biology*, **27**, 2974–2983.e2.

Chen, Y., **Li, W.**, **Turner, J.A.** & **Anderson, C.T.** (2021) PECTATE LYASE LIKE12 patterns the guard cell wall to coordinate turgor pressure and wall mechanics for proper stomatal function in Arabidopsis. *Plant Cell*, **33**, 3134–3150.

Cutler, S.R., **Ehrhardt, D.W.**, **Griffitts, J.S.** & **Somerville, C.R.** (2000) Random GFP::cDNA fusions enable visualization of subcellular structures in cells of Arabidopsis at a high frequency. *Proceedings of the National Academy of Sciences of the United States of America*, **97**, 3718–3723.

DeMichele, D.W. & **Sharpe, P.J.H.** (1973) An analysis of the mechanics of guard cell motion. *Journal of Theoretical Biology*, **41**, 77–96.

Engineer, C.B., **Hashimoto-Sugimoto, M.**, **Negi, J.**, **Israelsson-Nordström, M.**, **Azoulay-Shemer, T.**, **Rappel, W.J.** ***et al.*** (2016) CO_2 sensing and CO_2 regulation of stomatal conductance: advances and open questions. *Trends in Plant Science*, **21**, 16–30.

Forouzesh, E., **Goel, A.**, **MacKenzie, S.A.** & **Turner, J.A.** (2013) In vivo extraction of Arabidopsis cell turgor pressure using nanoindentation in conjunction with finite element modeling. *The Plant Journal*, **73**, 509–520.

Franks, P.J. & **Farquhar, G.D.** (2007) The mechanical diversity of stomata and its significance in gas-exchange control. *Plant Physiology*, **143**, 78–87.

Fujita, M. & **Wasteneys, G.O.** (2014) A survey of cellulose microfibril patterns in dividing, expanding, and differentiating cells of *Arabidopsis thaliana*. *Protoplasma*, **251**, 687–698.

Guo, X., **Wang, L.** & **Dong, J.** (2021) Establishing asymmetry: stomatal division and differentiation in plants. *New Phytologist*, **232**, 60–67.

Hayot, C.M., **Forouzesh, E.**, **Goel, A.**, **Avramova, Z.** & **Turner, J.A.** (2012) Viscoelastic properties of cell walls of single living plant cells determined by dynamic nanoindentation. *Journal of Experimental Botany*, **63**, 2525–2540.

Keynia, S., **Jaafar, L.**, **Zhou, Y.**, **Anderson, C.T.** & **Turner, J.A.** (2023) Stomatal opening efficiency is controlled by cell wall organization in *Arabidopsis thaliana* (E Bayer, Ed.). *PNAS Nexus*, **2**, pgad294.

Kinoshita, T., **Doi, M.**, **Suetsugu, N.**, **Kagawa, T.**, **Wada, M.** & **Shimazaki, K.** (2001) phot1 and phot2 mediate blue light regulation of stomatal opening. *Nature*, **414**, 656–660.

Kinoshita, T., **Emi, T.**, **Tominaga, M.**, **Sakamoto, K.**, **Shigenaga, A.**, **Doi, M.** ***et al.*** (2003) Blue-light- and phosphorylation-dependent binding of a 14-3-3 protein to phototropins in stomatal guard cells of broad bean. *Plant Physiology*, **133**, 1453–1463.

Li, W., **Keynia, S.**, **Belteton, S.A.**, **Afshar-Hatam, F.**, **Szymanski, D.B.** & **Turner, J.A.** (2022) Protocol for mapping the variability in cell wall mechanical bending behavior in living leaf pavement cells. *Plant Physiology*, **188**, 1435–1449.

Lopez-Anido, C.B., **Vatén, A.**, **Smoot, N.K.**, **Sharma, N.**, **Guo, V.**, **Gong, Y.** ***et al.*** (2021) Single-cell resolution of lineage trajectories in the Arabidopsis stomatal lineage and developing leaf. *Developmental Cell*, **56**, 1043–1055.e4.

Lucas, J.R., **Nadeau, J.A.** & **Sack, F.D.** (2006) Microtubule arrays and Arabidopsis stomatal development. *Journal of Experimental Botany*, **57**, 71–79.

Rui, Y. & **Anderson, C.T.** (2016) Functional analysis of cellulose and xyloglucan in the walls of stomatal guard cells of Arabidopsis. *Plant Physiology*, **170**, 1398–1419.

Rui, Y., **Chen, Y.**, **Yi, H.**, **Purzycki, T.**, **Puri, V.M.** & **Anderson, C.T.** (2019) Synergistic pectin degradation and guard cell pressurization underlie stomatal pore formation. *Plant Physiology*, **180**, 66–77.

Rui, Y., **Xiao, C.**, **Yi, H.**, **Kandemir, B.**, **Wang, J.Z.**, **Puri, V.M.** ***et al.*** (2017) POLYGALACTURONASE INVOLVED IN EXPANSION3 functions in seedling development, rosette growth, and stomatal dynamics in *Arabidopsis thaliana*. *The Plant Cell*, **29**, 2413–2432.

Sharma, N. (2017) Leaf clearing protocol to observe stomata and other cells on leaf surface. *Bio-Protocol*, **7**, e2538.

Weber, A., **Braybrook, S.**, **Huflejt, M.**, **Mosca, G.**, **Routier-Kierzkowska, A.L.** & **Smith, R.S.** (2015) Measuring the mechanical properties of plant cells by combining micro-indentation with osmotic treatments. *Journal of Experimental Botany*, **66**, 3229–3241.

Woolfenden, H.C., **Bourdais, G.**, **Kopischke, M.**, **Miedes, E.**, **Molina, A.**, **Robatzek, S.** ***et al.*** (2017) A computational approach for inferring the cell wall properties that govern guard cell dynamics. *The Plant Journal*, **92**, 5–18.

Yi, H., **Chen, Y.** & **Anderson, C.T.** (2022) Turgor pressure change in stomatal guard cells arises from interactions between water influx and mechanical responses of their cell walls. *Quantitative Plant Biology*, **3**, e12.

Zhao, L. & **Sack, F.D.** (1999) Ultrastructure of stomatal development in Arabidopsis (Brassicaceae) leaves. *American Journal of Botany*, **86**(7), 929–939.